Article

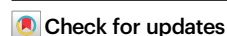# Anti-PD1 based precision induction therapy in unresectable stage III non-small cell lung cancer: a phase II umbrella clinical trial

Chengxiang Yi [1,5], Dongliang Bian [1,5], Jue Wang[1,5], Shiqi Hu[2,5], Liangdong Sun[1], Yilv Yan[1], Suyu Wang[1], Ziyun Shen[1], Huansha Yu[3], Yong Yang [1], Yirui Zhou[1], Xiaogang Liu[1], Nan Song[1], Yuming Zhu[1], Deping Zhao[1], Gening Jiang[1], Liang Duan[1], Wenxin He [1], Dong Xie[1,6] ✉, Jie Dai [1,6] ✉, Lele Zhang [4,6] ✉ & Peng Zhang [1,2,6] ✉

The efficacy and safety of induction-immunotherapy followed by surgery for unresectable Stage III non-small cell lung cancer (NSCLC) remain challenging. In this open-label, single-center, phase II clinical umbrella trial (ChiCTR2000035367), 100 unresectable Stage III NSCLC patients are enrolled. Patients with PD-L1 expression ≥ 50% but contraindications to anti-angiogenic therapy receive immuno-monotherapy. Patients with PD-L1 expression ≥ 1% and no contraindications to anti-angiogenic therapy receive immunotherapy plus anti-angiogenesis therapy. Patients with PD-L1 expression between 1% and 49%, contraindications to anti-angiogenic therapy, or negative/unknown PD-L1 expression receive chemoimmunotherapy. The primary endpoint is the major pathological response (MPR) rate. Among 47 surgically-treated patients, the MPR rate is 61.7% (95% confidence interval [CI]: 46.4%-75.5%), achieving the prespecified endpoint. For secondary endpoints, the objective response rate for all patients is 54.0% (95% CI: 43.7-64.0). The median event-free survival is 29.9 months (95% CI: 17.0-42.7). Most common adverse event is anemia (49.0%). Exploratory transcriptomic analyses reveal Bone Marrow Stromal Cell Antigen 1 (BST1) as a promising biomarker for response to chemoimmunotherapy. Generally, for unresectable stage III NSCLC patients, anti-PD1 based induction-therapy according to PD-L1 expression and contraindication to antiangiogenic therapy followed by surgery is a feasible option.

Lung cancer is the most common type of cancer and the leading cause of cancer-related mortality globally, resulting in approximately 1.8 million deaths annually[1]. Non-small cell lung cancer (NSCLC) emerged as the predominant pathological subtype, constituting the majority of cases[2]. Notably, over 15% of NSCLC diagnoses pertain to individuals in the locally advanced stage (Stage III)[3]. The 5-year overall survival (OS) rates for stage III NSCLC vary significantly, ranging from 36% for stage IIIA to 13% for stage IIIC[2]. The diverse composition of this patient

[1]Department of Thoracic Surgery, Shanghai Pulmonary Hospital, School of Medicine, Tongji University, Shanghai 200433, China. [2]Department of Thoracic Surgery, The First Affiliated Hospital of Wenzhou Medical University, Wenzhou, China. [3]Experimental Animal Center, Shanghai Pulmonary Hospital, School of Medicine, Tongji University, Shanghai 200433, China. [4]Central Laboratory, Shanghai Pulmonary Hospital, School of Medicine, Tongji University, Shanghai 200433, China. [5]These authors contributed equally: Chengxiang Yi, Dongliang Bian, Jue Wang, Shiqi Hu. [6]These authors jointly supervised this work: Dong Xie, Jie Dai, Lele Zhang, Peng Zhang. ✉e-mail: xiedong@tongji.edu.cn; daijie@tongji.edu.cn; zhanglele@tongji.edu.cn; zhangpeng1121@tongji.edu.cn

cohort, exhibiting a range of T- and N-descriptors upon diagnosis, necessitates a comprehensive array of treatment strategies[4].

In 2022, multiple Phase III randomized trials (namely, CheckMate 816, CheckMate 77 T, KEYNOTE-671, and NEOTORCH) revealed that, in comparison with neoadjuvant chemotherapy, the incorporation of neoadjuvant programmed cell death protein 1 (PD-1) immune checkpoint inhibitors in conjunction with chemotherapy yields notable enhancements in the major pathologic response (MPR), pathologic complete response (pCR), and event-free survival (EFS) among patients with locally advanced NSCLC[5–8]. Therefore, neoadjuvant chemoimmunotherapy followed by complete surgery has been recommended as the standard treatment for resectable Stage III NSCLC without EGFR/ALK mutations[9–13].

For unresectable Stage III NSCLC, the PACIFIC trial proposed a novel treatment approach that involves concurrent chemoradiotherapy (cCRT) followed by a year of consolidation durvalumab, which improved the 5-year OS to 42.9%[14]. Therefore, PACIFIC mode has been recommended as the standard treatment for patients with unresectable Stage III NSCLC according to National Comprehensive Cancer Network (NCCN) guideline[15]. In 2022, a single-arm, phase II clinical trial (LungMate-002) demonstrated that 65.8% patients with unresectable NSCLC were converted to resectable disease after neoadjuvant chemoimmunotherapy[16]. A limited number of retrospective studies have also revealed the efficacy and safety of neoadjuvant chemoimmunotherapy for patients with potentially resectable Stage III NSCLC without EGFR/ALK mutations[17]. These findings provide valuable insights into the potential benefits of preoperative chemoimmunotherapy for patients with initially unresectable stage III NSCLC.

In addition, a single-arm, Phase II clinical trial demonstrated the promising efficacy and safety of neoadjuvant camrelizumab plus apatinib (PD-1 inhibitor plus angiogenesis inhibitor) for patients with resectable locally advanced NSCLC with positive PD-L1 expression[18]. Many studies have shown that VEGF inhibitors exert an immune-enhancing effect[19], and several preclinical studies have shown that immunotherapy plus VEGF-targeted therapy can enhance the effectiveness of immunotherapy[20,21]. These results demonstrated the potential value of the combined use of PD-1 and angiogenesis inhibitors in neoadjuvant therapy.

This Phase II clinical umbrella trial aimed to assess the efficacy and safety of anti-PD1-based precision induction therapies in patients with unresectable stage III NSCLC selected based on tumor PD-L1 expression and contraindications to antiangiogenic therapy. Patients received one of these three treatment regimens: anti-PD1 plus anti-angiogenic therapy, anti-PD1 therapy combined with chemotherapy, or anti-PD1 induction therapy. The trial met the primary end point with an MPR rate of 61.7%. Moreover, our exploratory molecular analyses offer insights into potential biomarkers for further optimization of treatment strategies in this specific patient cohort.

Results

Baseline characteristics

Between January 21, 2021, and March 1, 2023, 108 patients were screened and 100 were enrolled in this trial (Fig. 1). All 100 participants were divided into two subgroups, the Chemo and Chemo-free subgroups.

In the Chemo-free subgroup ($n = 21$), 15 patients with positive (PD-L1 ≥ 1%) expression received induction sintilimab (anti-PD1) combined with IBI305 (a biosimilar to the anti-VEGF monoclonal antibody bevacizumab). The remaining 6 participants, characterized by high PD-L1 expression (PD-L1 ≥ 50%) but contraindications for IBI305, were treated with sintilimab monotherapy (Supplementary Table 1). In the Chemo subgroup (receiving induction sintilimab combined with chemotherapy), 68 participants had negative (PD-L1 < 1%, $n = 21$) or nonaccessible PD-L1 expression ($n = 47$) and the remaining 11 participants

had low PD-L1 expression (50% > PD-L1 ≥ 1%) and were contraindicated for IBI305 (Fig. 1, Supplementary Fig. 1a, and Supplementary Table 1). A total of 47 patients who underwent surgery were included in the primary endpoint analysis. The baseline characteristics of the participants are listed in Table 1.

Among the 100 patients, the average age at diagnosis was 62.9 years (range, 40.0–82.0 years), with a predominance of male participants (93/100) and smokers (90/100). Furthermore, 76 patients exhibited an ECOG performance status of 0 (76/100). Moreover, 44, 48, and 8 patients were in clinical Stage IIIA, IIIB, and IIIC, respectively; notably, N3 node stage disease was identified in 15 participants. The participants received induction therapy for an average of 3.4 cycles (Tables 1 and 2).

Efficacy

The MPR rate in surgically treated patients ($n = 47$) was 61.7% (95% CI: 46.4%–75.5%), which met the prespecified primary endpoint in this trial. Additionally, 18 (38.3%, 95% CI: 24.5%–53.6%) of the 47 patients achieved a pCR (Supplementary Fig. 1b and Table 2).

The rates of pCR and MPR were numerically higher among smokers (42.9% vs. 0.0% and 64.3% vs. 40.0%, $P = 0.141$ and 0.291, respectively). However, it is important to note the relatively small sample size of non-smokers ($n = 5$). In contrast, the overall response rates (ORRs) were comparable between smokers and never-smokers (53.3% vs. 60%, $P = 0.688$). In the pathological subgroups, similar pCR rates and MPR rates were noted between different pathological types (42.3% vs. 33.3% and 61.5% vs. 61.9%, $P = 0.529$ and 0.980 for LUSC vs. non-LUSC). Furthermore, the ORR demonstrated comparable efficacy between LUSC and non-LUSC patients (55.6% vs. 52.2%, $P = 0.735$, Supplementary Fig. 1b, c).
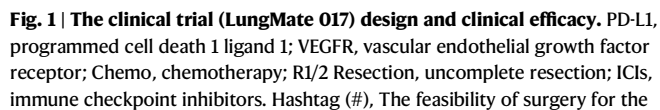
Fifty-eight participants in this trial were assessed for resectable disease after induction treatment by multidisciplinary team (MDT). Among these patients, 47 participants received radical surgery after induction treatment, 8 patients did not undergo surgery due to adverse events, and the remaining 3 did not undergo surgery due to patient choice (Supplementary Tables 2 and 3). Among the 47 patients, 30 patients (63.8%) underwent video-assisted thoracoscopic surgery (VATS) and 38 patients (80.8%) underwent lobectomy. All 47 patients (100%) underwent R0 resection. The median drainage tube removal time was 10.0 (IQR: 5.0-15.8) days, and the duration of postoperative hospital stay was 5.0 (IQR: 4.0-8.0) days (Supplementary Table 3).

Radiological efficacy

Among the 100 enrolled patients, 92 underwent treatment efficacy assessment after induction therapy (3 patients did not undergo posttreatment assessments because of Grade 5 adverse events during the study period, one patient discontinued due to Grade 5 psychiatric disturbance, and 4 patients did so because of patient choice). Among the population for intention-to-treat analysis ($n = 100$), 2 patients (2.0%) achieved a radiological completed response (CR), 52 patients (52.0%) achieved a radiological partial response (PR), 37 patients (37.0%) had radiological stable disease (SD), and 1 patient (1.0%) experienced radiological progressive disease (PD) after induction therapy. An objective response (CR and PR) was achieved in 54 patients (54.0%; 95% CI: 43.7%–64.0%, Supplementary Fig. 1c and Supplementary Table 4). Among the never smokers ($n = 10$) and the LUSC ($n = 54$) subgroup, an objective response was achieved in 6 patients (60.0%; 95% CI: 26.2%–87.8%) and 30 patients (55.6%; 95% CI: 41.4%–69.1%), respectively (Supplementary Fig. 1c).

Subgroup analysis

In the Chemo-free subgroup, 21 patients were initially deemed unresectable at diagnosis, and nine of these patients underwent radical surgery following induction therapy, resulting in a conversion rate to

Fig. 1 | The clinical trial (LungMate 017) design and clinical efficacy. PD-L1, programmed cell death 1 ligand 1; VEGFR, vascular endothelial growth factor receptor; Chemo, chemotherapy; R1/2 Resection, uncomplete resection; ICIs, immune checkpoint inhibitors. Hashtag (#), The feasibility of surgery for the patient (Surgery performed at an external institution) was assessed by our MDT team based on radiological data before (our hospital) and after (external institution) induction therapy.

surgery of 42.9%. The mean interval between the last dosage of induction treatment and surgery was 49.2 days (95% CI: 40.3 to 59.8, Fig. 2a). Furthermore, the MPR rate in the Chemo-free subgroup (*n* = 9) was 55.6% (95% CI: 21.2%–86.3%, Fig. 2b). The MPR rates were 100.0% (95% CI: 15.8%–100.0%,) and 42.9% (95% CI: 9.9%–81.6%) for ICI monotherapy (*n* = 2) and ICI plus IBI305 (*n* = 7) respectively. Except for one participant who refused to be assessed in our center after induction therapy, the radiological disease control rate (DCR) in the remaining 20 patients was 100%.

In the Chemo subgroup, 79 patients were initially deemed unresectable at diagnosis. Among them, 38 patients underwent radical surgery following induction therapy, resulting in a conversion rate to surgery of 48.1%. The mean interval between induction and surgery was 40.9 (95% CI, 35.7 to 45.8) days (Fig. 3a). The MPR rate was 63.2%

(24 out of 38 patients underwent surgery, 95% CI: 46.0%–78.2%, Fig. 3b). Among the 79 patients (seven patients without re-evaluation data), 2 patients (2.5%) achieved CR, 40 patients (50.6%) achieved PR, 29 patients (36.7%) had SD, and 1 patient (1.3%) had PD. Among the 47 patients with non-accessible PD-L1 status (excluding five without re-evaluation data), 26 (55.3%) achieved PR, 15 (31.9%) had SD, and 1 (2.1%) showed PD. The MPR rate among the 19 patients with non-accessible PD-L1 status who underwent surgery was 78.9% (95% CI: 54.4%–93.9%).

Survival analysis

The median follow-up time was 25.4 (95% CI: 22.6–28.3) months at the time of data cut-off (April 15, 2024). A total of 71 participants (71.0%) were alive. The estimated percentage of participants who were alive was 83.5% (95% CI, 74.4 to 89.5) at 12 months and 69.0% (95% CI, 57.8 to

Table 1 | Characteristics of the patients at baseline

Characteristic	Primary analysis set		Intention-to-treat analysis set	
	Chemo-free (n = 9, %)	Chemo (n = 38, %)	Chemo-free (n = 21, %)	Chemo (n = 79, %)
Age, years, mean ± SD [a]	63.78 ± 6.78	61.50 ± 7.99	61.90 ± 9.92	63.14 ± 8.57
Sex				
Male	9 (100.0)	34 (89.5)	19 (90.5)	74 (93.7)
Female	0 (0.0)	4 (10.5)	2 (9.5)	5 (6.3)
ECOG performance status				
0	9 (100.0)	27 (71.1)	18 (85.7)	58 (73.4)
1	0 (0.0)	11 (28.9)	3 (14.3)	21 (26.6)
PD-L1 expression level				
≥ 50%	3 (33.3)	0 (0.0)	8 (38.1)	0 (0.0)
1% ~ 50%	6 (66.7)	6 (15.8)	13 (61.9)	11 (13.9)
<1%	0 (0.0)	13 (34.2)	0 (0.0)	21 (26.6)
Unknown	0 (0.0)	19 (50.0)	0 (0.0)	47 (59.5)
Smoking status				
Never	1 (11.1)	4 (10.5)	3 (14.3)	7 (8.9)
Current	3 (33.3)	26 (68.4)	11 (52.3)	54 (68.4)
Former (≥1 y)	5 (55.6)	8 (21.1)	7 (33.3)	18 (22.8)
Pack-years, median [IQR] [a]	40.0 [23.8, 52.5]	30.0 [20.0, 48.8]	43.8 [23.1, 60.0]	36.0 [21.9, 50.0]
MTD at diagnosis, mm, median [IQR]	29.0 [25.0, 50.0]	43.0 [31.8, 61.3]	43.0 [32.0, 56.0]	47.0 [38.0, 68.5]
N stage at diagnosis				
N0	0 (0.0)	0 (0.0)	0 (0.0)	3 (3.8)
N1	2 (22.2)	3 (7.9)	3 (14.3)	13 (16.5)
N2	5 (55.6)	30 (78.9)	12 (57.1)	54 (68.4)
N3	2 (22.2)	5 (13.2)	6 (28.6)	9 (11.4)
cTNM stage at diagnosis				
IIIA	4 (44.4)	20 (52.6)	5 (23.8)	39 (49.4)
IIIB	4 (44.4)	14 (36.8)	14 (66.7)	34 (43.0)
IIIC	1 (11.1)	4 (10.5)	2 (9.5)	6 (7.6)
Histologic features				
Non-LUSC[a]	2 (22.2)	20 (52.6)	6 (28.6)	40 (50.6)
LUSC	7 (77.8)	18 (47.4)	15 (71.4)	39 (49.4)

[a]MTD maximum tumor dimension, LUSC lung squamous cell carcinoma, IQR interquartile range, SD standard deviation.

Table 2 | Efficacy evaluation

	Total (n = 47, %)	Chemo-free (n = 9, %)	Chemo (n = 38, %)
MTD pre, mm, median [IQR] [a]	21.4 [12.5, 32.5]	21.4 [15.0, 32.0]	21.2 [12.0, 32.7]
PLN pre, median [IQR] [a]	0.0 [0.0, 1.0]	1.0 [0.0, 2.0]	0.0 [0.0, 1.0]
cTNM stage following induction therapy			
O/I	18 (38.3)	2 (22.2)	16 (42.1)
II	11 (23.4)	3 (33.3)	8 (21.1)
III	18 (38.3)	4 (44.4)	14 (36.8)
MTD post, mm, median [IQR] [a]	20.0 [0.0, 30.0]	21.0 [0.0, 32.0]	19.5 [0.0, 29.5]
PLN post, median [IQR] [a]	0.0 [0.0, 1.5]	1.0 [0.0, 2.0]	0.0 [0.0, 1.0]
ypN downstaging	37 (78.7)	6 (66.7)	31 (81.6)
ypTNM			
O/I	27 (57.4)	4 (44.4)	23 (60.5)
II	6 (12.8)	1 (4.8)	5 (13.2)
III	14 (29.8)	4 (44.4)	10 (26.3)
Residual tumor cell, % (range)	19.0 (0.0-90.0)	24.4 (0.0-80.0)	20.0 (0.0-90.0)
Pathologic regression			
pCR [a]	18 (38.3)	3 (33.3)	15 (39.5)
MPR [a]	29 (61.7)	5 (55.6)	24 (63.2)

[a]MTD pre maximum tumor dimension measured prior to surgery following induction therapy, MTD post maximum tumor dimension based on the surgical pathological report following induction therapy, PLN pre positive lymph node number prior to surgery following induction therapy, PLN post the number of positive lymph nodes based on the surgical pathological report following induction therapy, IQR interquartile range, pCR pathological complete response, MPR major pathological response.

77.8) at 24 months. The median OS was not reached (Supplementary Fig. 1d). A total of 29 participants died during the study, with 16 patients experiencing tumor recurrence. Among these, ten deaths were directly attributed to lung cancer. At 12 months, the estimated percentage of EFS was 78.5% (95% CI, 69.0 to 85.4); at 2 years, the corresponding value was 53.5% (95% CI, 41.8 to 63.8). The median EFS was 29.9 months (95% CI, 17.2 to 42.5, Supplementary Fig. 1e). Tumor recurrence was observed in 27 patients, with 19 experiencing locoregional recurrence (17 in the Chemo subgroup) and 9 developing distant recurrence (all in the Chemo subgroup, Supplementary Table 5)

In the Chemo-free subgroup, the median OS and EFS were not reached. The one-year OS and EFS rates were both 95.0% (95% CI, 69.5 to 99.3, Supplementary Fig. 2a-b). In the Chemo subgroup, the median EFS was estimated at 23.4 months (95% CI: 15.4 to 31.4), whereas the median OS was not determined; the one-year OS rate was 80.4% (95% CI: 69.6 to 87.7) and the one-year EFS rate was 74.2% (95% CI:62.9 to 82.5, Supplementary Fig. 2c-d). Interestingly, for patients who underwent sequential surgery, the estimated OS and EFS rates were 93.5%

(95% CI, 81.2 to 97.9) and 89.2% (95% CI, 75.9 to 95.3), respectively, at 12 months and 81.0% (95% CI, 65.2 to 90.1) and 66.1% (95% CI, 49.1 to 78.6), respectively, at 24 months (Supplementary Fig. 2e-f). However, for patients who did not receive sequential surgery, the estimated OS and EFS rates were 74.3% (95% CI, 59.8 to 84.2) and 69.0% (95% CI, 54.4 to 79.7), respectively, at 12 months, and 57.6% (95% CI, 41.0 to 71.0) and 40.9% (95% CI, 25.1 to 56.0), respectively, at 24 months (Supplementary Fig. 2g-h).

Safety
Adverse events of any cause were observed in 92.0% of the patients within the total cohort, with rates of 76.2% in the Chemo-free subgroup and 96.2% in the Chemo subgroup. Treatment-related adverse events (TRAEs) were observed in 90% of patients and the most common TRAEs were anemia (49%), alopecia (46%) and neutropenia (46%). The incidence of Grade ≥ 3 TRAEs was 35.0% in the total cohort, with 14.3% in the Chemo-free subgroup and 40.5% in the Chemo subgroup (Table 3). Treatment-related deaths were due to pneumonitis, heart failure and hemorrhage of digestive tract after myelosuppression (only in the Chemo subgroup). Overall, the incidence of immune-related adverse events (irAEs) was 17.0%, and events were mainly of Grade 1 or 2. The most common irAEs were pneumonitis (8.0%) and hypothyroidism (2.0%). Two patients in the Chemo-subgroup died due to immune-related interstitial lung disease and pneumonitis (Supplementary Table 6). Further, the incidence of surgery-related adverse events (srAEs) was low, and events were mainly of Grade 1 or 2. The most common srAEs were postoperative pleural effusion (29.8%) and prolonged air leakage (8.5%); one patient in the Chemo-free subgroup had Grade 3 bronchopulmonary fistula. Only one patient in the Chemo subgroup died due to postoperative hemoptysis, which was determined to be unrelated to the trial drugs by the investigator (Supplementary Table 7).
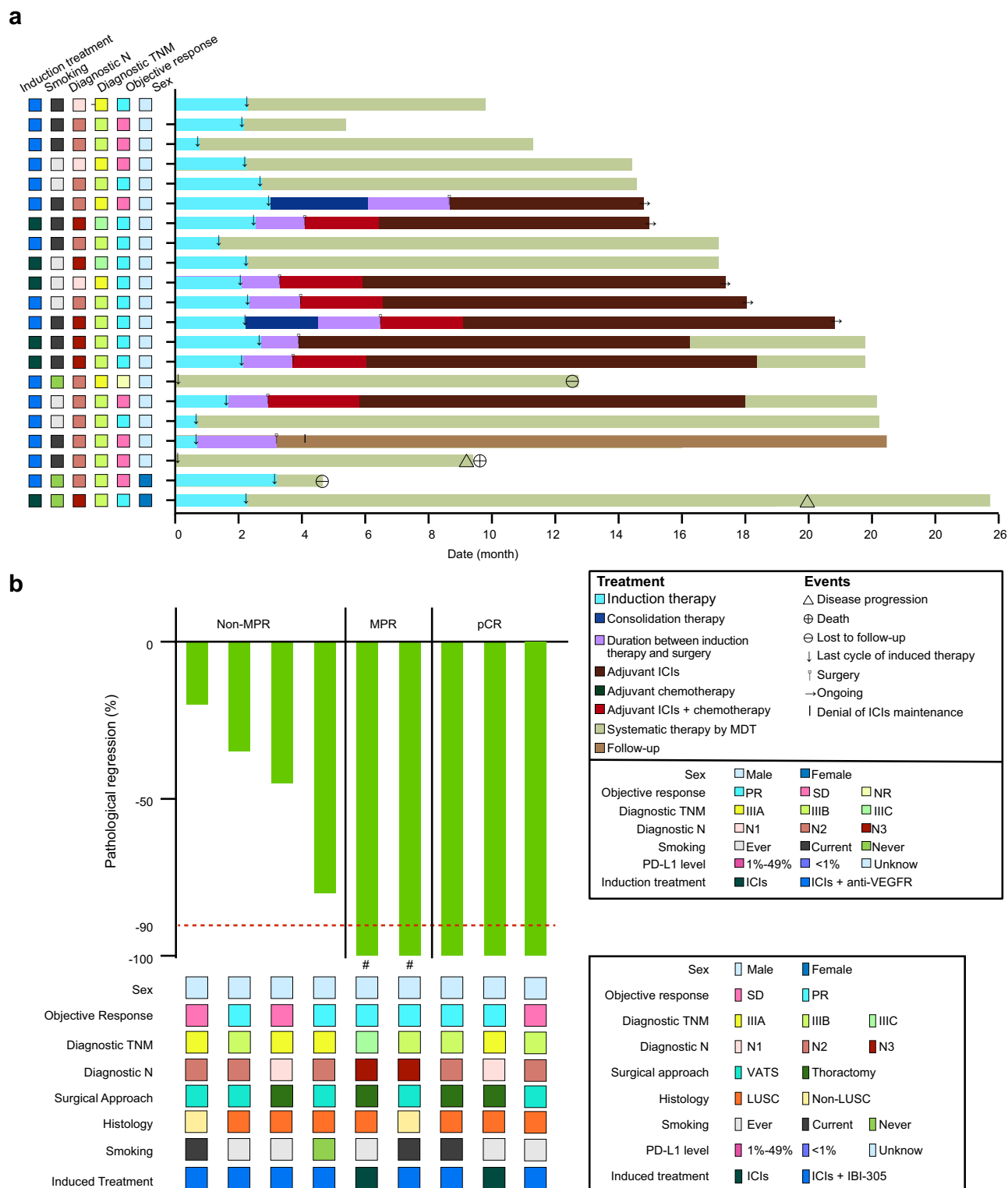
a

b

Fig. 2 | Tumor responses in the Chemo-free subgroup. a Swimming plot showing duration of treatment and clinical events occurrence in Chemo-free subgroup (*n* = 21). **b** Waterfall plot of pathologic regression in Chemo-free subgroup patients with surgical resection after induction treatment (*n* = 9). RECIST response evaluation criteria in solid tumors, NR, not re-evaluation, PR partial response, SD stable disease,

MPR major pathologic response, ICIs, immune checkpoint inhibitors, VATS, video-assisted thoracoscopic surgery, VEGFR, vascular endothelial growth factor receptor; MDT, multidisciplinary team; LUSC, Lung squamous cell carcinoma. Hashtag (#), represents pathological result showed -100% pathological regression ratios but with positive sampled lymph nodes. Source data are provided as a Source Data file.

Exploratory endpoint

We then analyzed the genomic and transcriptomic features associated with the treatment response. We explored more accurate biomarkers to stratify and improve the efficacy of induction immunotherapy in patients with unresectable Stage III NSCLC (Supplementary Fig. 3a).

Genomic biomarker analysis for precision induction therapy

The genomic analysis included 27 patients in the Chemo subgroup and 8 patients in the Chemo-free subgroup (who received anti-PD1 + anti-VEGFR, Supplementary Fig. 3b). The Chemo-free subgroup included 5 non-LUSC patients and 3 LUSC patients, with 3 showing a response to
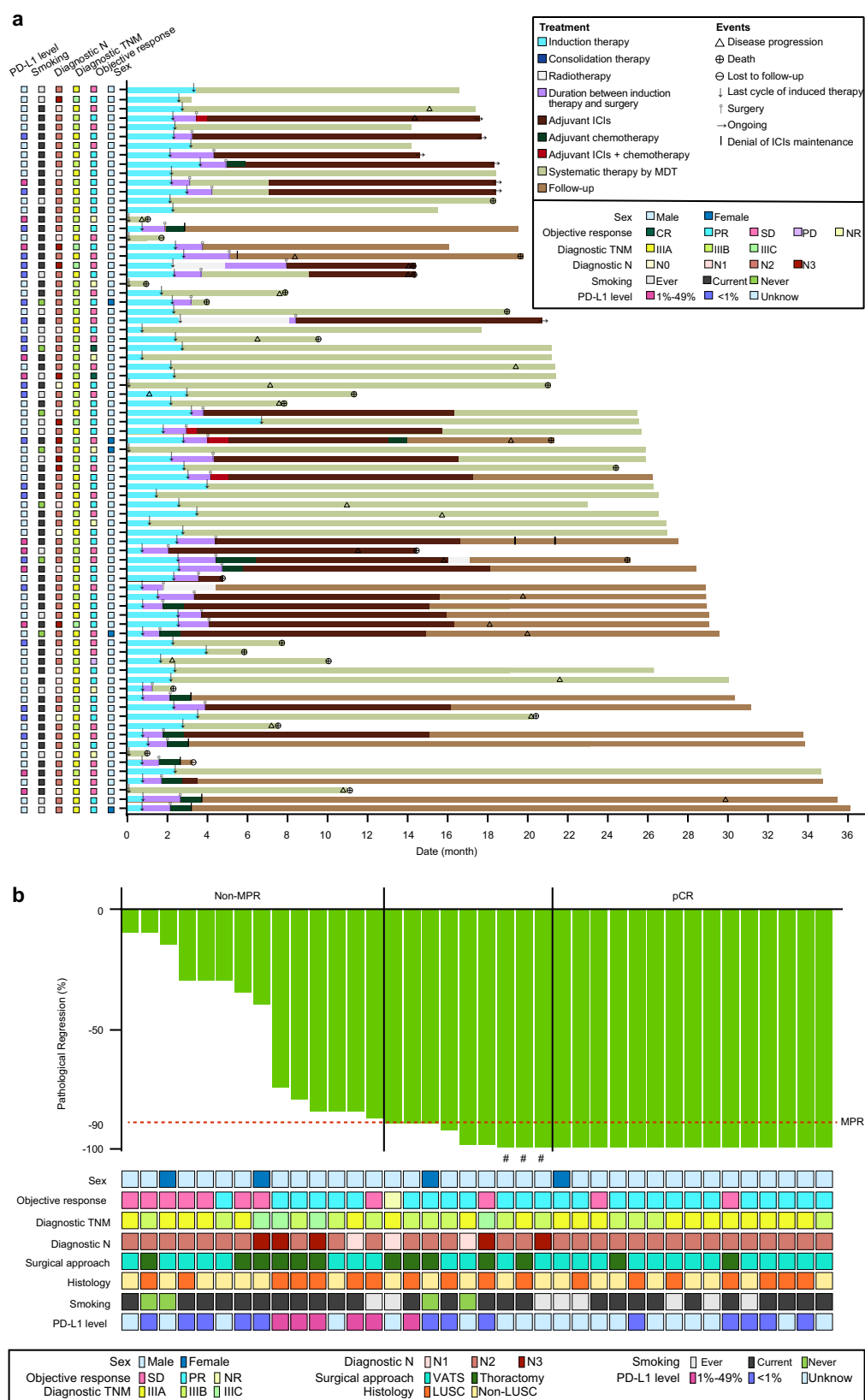
Fig. 3 | Tumor responses in the Chemo subgroup. a Swimming plot showing the duration of treatment and clinical events occurrence in the Chemo subgroup ($n = 79$). **b** Waterfall plot of pathologic regression in the Chemo subgroup patients with surgical resection after induction treatment ($n = 38$). RECIST response evaluation criteria in solid tumors, NR, not re-evaluation, PR partial response, SD stable disease, MPR major pathologic response, ICIs, immune checkpoint inhibitors, VATS, video-assisted thoracoscopic surgery, VEGFR, vascular endothelial growth factor receptor; MDT, multidisciplinary team; LUSC, Lung squamous cell carcinoma. Hashtag (#), represents pathological result showed -100% pathological regression ratios but with positive sampled lymph nodes. Source data are provided as a Source Data file.

Table 3 | Treatment related adverse events

| Type of event	Total (n = 100)		Chemo-free (n = 21)		Chemo (n = 79)	
	All grades (%)	Grade ≥ 3 (%)	All grades (%)	Grade ≥ 3 (%)	All grades (%)	Grade ≥ 3 (%)
Total	90 (90.0)	35 (35.0)	15 (71.4)	3 (14.3)	75 (94.9)	32 (40.5)
Anemia	49 (49.0)	1 (1.0)	4 (19.0)	0 (0.0)	45 (57.0)	1 (1.3)
Alopecia	46 (46.0)	18 (18.0)	2 (9.5)	0 (0.0)	44 (55.7)	18 (22.8)
Neutropenia	46 (46.0)	16 (16.0)	2 (9.5)	1 (4.8)	44 (55.7)	15 (19.0)
Leukopenia	41 (41.0)	5 (5.0)	2 (9.5)	0 (0.0)	39 (49.4)	5 (6.3)
ALT increased [a]	24 (24.0)	3 (3.0)	4 (19.0)	0 (0.0)	20 (25.3)	3 (3.8)
AST increased [a]	18 (18.0)	2 (2.0)	5 (23.8)	0 (0.0)	13 (16.5)	2 (2.5)
Thrombocytopenia	15 (15.0)	3 (3.0)	1 (4.8)	0 (0.0)	14 (17.7)	3 (3.8)
Hyperglycemia	15 (15.0)	0 (0.0)	4 (19.0)	0 (0.0)	11 (13.9)	0 (0.0)
Fatigue	11 (11.0)	0 (0.0)	2 (9.5)	0 (0.0)	9 (11.4)	0 (0.0)
Hemoptysis	9 (9.0)	3 (3.0)	4 (19.0)	3 (14.3)	5 (6.3)	0 (0.0)
Fever	9 (9.0)	1 (1.0)	2 (9.5)	0 (0.0)	7 (8.9)	1 (1.3)
Lymphopenia	9 (9.0)	0 (0.0)	0 (0.0)	0 (0.0)	9 (11.4)	0 (0.0)
Cough	8 (8.0)	3 (3.0)	2 (9.5)	1 (4.8)	6 (7.6)	2 (2.5)
Creatinine increase	8 (8.0)	0 (0.0)	2 (9.5)	0 (0.0)	6 (7.6)	0 (0.0)
Peripheral neuropathy	7 (7.0)	0 (0.0)	0 (0.0)	0 (0.0)	7 (8.9)	0 (0.0)
Rash	6 (6.0)	1 (1.0)	1 (4.8)	0 (0.0)	5 (6.3)	1 (1.3)
Hypertriglyceridemia	5 (5.0)	0 (0.0)	2 (9.5)	0 (0.0)	3 (3.8)	0 (0.0)
Bacterial pneumonitis	5 (5.0)	4 (4.0)	2 (9.5)	1 (4.8)	3 (3.8)	3 (3.8)
Hyponatremia	4 (4.0)	0 (0.0)	0 (0.0)	0 (0.0)	4 (5.1)	0 (0.0)
Hypokalemia	4 (4.0)	0 (0.0)	0 (0.0)	0 (0.0)	4 (5.1)	0 (0.0)
Vomiting	4 (4.0)	0 (0.0)	0 (0.0)	0 (0.0)	4 (5.1)	0 (0.0)
Hypoalbuminemia	4 (4.0)	0 (0.0)	1 (4.8)	0 (0.0)	3 (3.8)	0 (0.0)
Decreased appetite	4 (4.0)	0 (0.0)	1 (4.8)	0 (0.0)	3 (3.8)	0 (0.0)
Constipation	3 (3.0)	0 (0.0)	0 (0.0)	0 (0.0)	3 (3.8)	0 (0.0)
Heart failure	2 (2.0)	1 (1.0)	0 (0.0)	0 (0.0)	2 (2.5)	1 (1.3)
Dyspepsia	2 (2.0)	0 (0.0)	2 (9.5)	0 (0.0)	0 (0.0)	0 (0.0)
Arthralgia	1 (1.0)	1 (1.0)	0 (0.0)	0 (0.0)	1 (1.0)	1 (1.0)
Diarrhea	1 (1.0)	0 (0.0)	0 (0.0)	0 (0.0)	1 (1.3)	0 (0.0)
Cerebral arterial insufficiency	1 (1.0)	0 (0.0)	0 (0.0)	0 (0.0)	1 (1.3)	0 (0.0)
Nausea	1 (1.0)	0 (0.0)	0 (0.0)	0 (0.0)	1 (1.3)	0 (0.0)

[a]*ALT* alanine transaminase, *AST* aspartate aminotransferase.
See also Tables S6–S7.

immunotherapy (PR) and 5 exhibiting no response (SD). The Chemo subgroup included 13 non-LUSC patients and 14 LUSC patients, with 17 responding to immunotherapy (PR) and 8 showing no response (SD). The most prevalent somatic variations were TP53 (60%), LRP1B (17%) and NOTCH1 (14%). Interestingly, an increased clinical benefit of immunotherapy (Chemo-free subgroup) was observed in patients with TP53 mutations (100.0% vs. 40% for response vs. non-response, $P = 0.196$, Supplementary Fig. 3c). Additionally, patients with good immunotherapy responses presented a numerically greater TMB than non-responders did, although no statistically significant difference was observed in the Chemo-free subgroup ($P = 0.250$; Supplementary Fig. 3d). However, in the Chemo subgroup, we did not identify this difference between responders and non-responders (Supplementary Fig. 3e). However, these observations are preliminary and based on observed trends, and further research is needed to validate these findings.

BST1 is a promising biomarker for patients receiving chemoimmunotherapy

To refine patient stratification for chemoimmunotherapy applications, we conducted an in-depth analysis to characterize the intrinsic transcriptomic features of baseline biopsy sample based on RNA sequencing data. Using radiological response as a criterion, we identified 357 upregulated genes in responders (13 patients who achieved CR/PR following induction therapy, compared to 11 non-responders who exhibited SD/PD, Fig. 4a, b). Notably, the radiologic response demonstrated robust predictive value for the pathologic response (Supplementary Fig. 4a). Upon assessing pathologic responses, we identified 749 upregulated genes ($P < 0.05$ & $\log2FC > 1$) in patients exhibiting an MPR (6 Non-MPR vs. 6 MPR), with only 85 genes showing upregulation in both comparative analyses (Supplementary Fig. 4b–d). Among these 85 genes, further selection was conducted based on prognostic analyses for EFS and OS (Supplementary Data 1 and Fig. 4c, d). Only two genes, *BST1* (Bone Marrow Stromal Cell Antigen 1) and *CDX2*, met our criteria (Supplementary Fig. 4e). Because CDX2 is a key transcription factor that controls intestinal fate and is associated with colorectal cancer[22], and *BST1* demonstrated superior predictive ability in survival analysis and ROC results (Fig. 4e), we screened *BST1* as the most suitable biomarker. We subsequently validated the predictive potential of BST1 as a marker for immunotherapy efficacy at the protein level. Through immunohistochemistry (IHC) analysis, we observed increased BST1 protein levels within the tumors of responders, indicating its consistent predictive efficacy for the immunotherapy response (Fig. 4f–h). Additionally, patients with high BST1 IHC scores demonstrated increased OS and EFS (Fig. 4i, j).
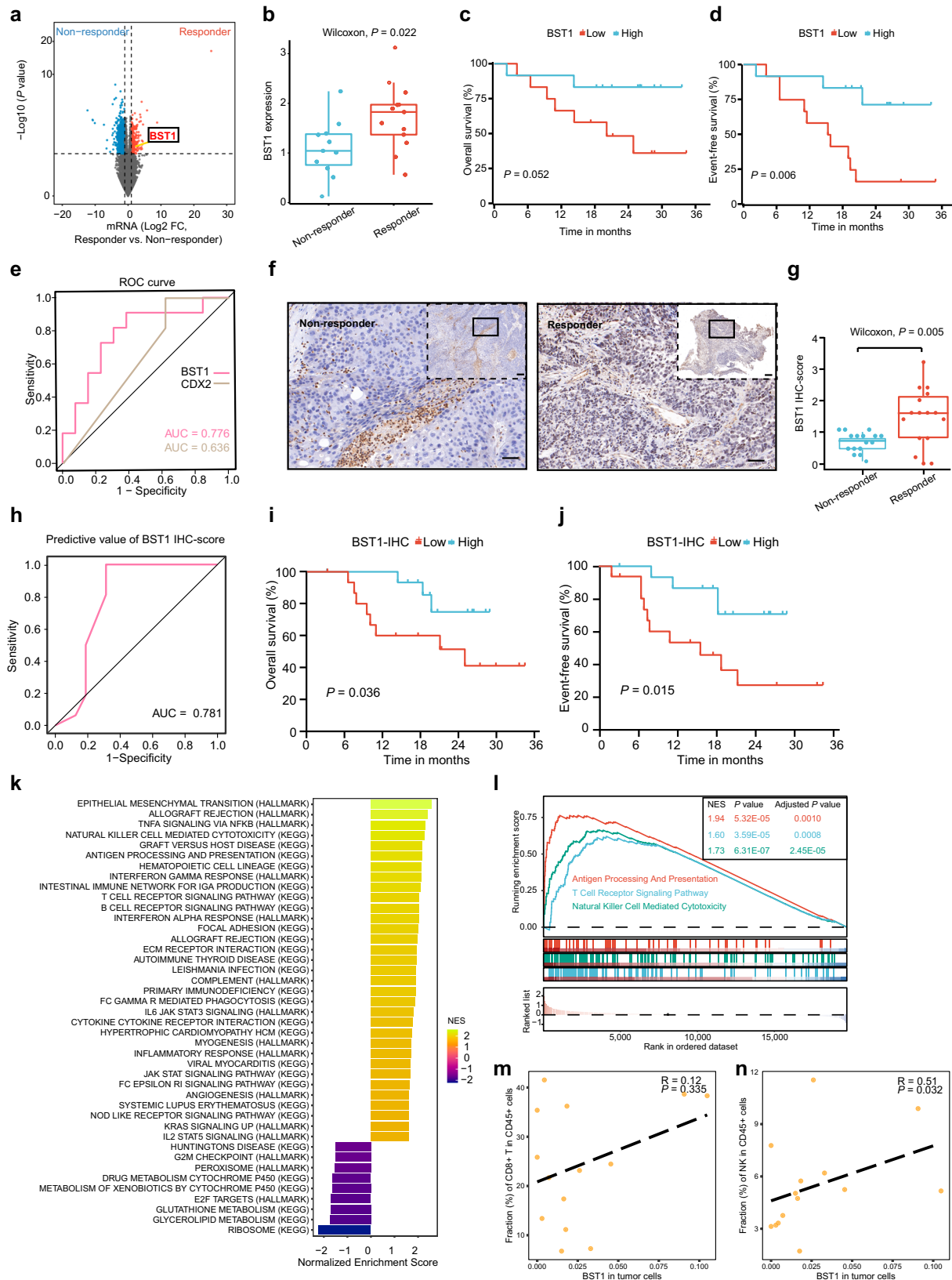
We extended our investigation to identify the most significantly enriched functional terms that differentiated responders from non-responders via gene set enrichment analysis (GSEA). Notably, pathways such as "Natural Killer (NK) Cell Mediated Cytotoxicity", "Interferon Gamma Response" and others were found to be significantly enriched (Fig. 4k). Furthermore, GSEA unveiled significant enrichment

of TCR, antigen presentation and NK cell-mediated cytotoxicity pathways in BST1-high tumors (Fig. 4l). Moreover, our data revealed a consistent positive correlation between BST1 expression and immune infiltration (Supplementary Fig. 4f-h). Because the study population was recruited exclusively from China, we further analyzed the differences in the expression of *BST1* across Asian versus non-Asian patients

Fig. 4 | BST1 is a promising biomarker for chemoimmunotherapy response in patients with negative or low-level PD-L1 expression. a Volcano plot of gene log2 fold change (x-axis) between chemoimmunotherapy-responders (PR, $n = 13$) and non-responders (SD, $n = 11$) baseline tumor versus -log10 P value (y-axis) determined by DEseq2. **b** Bar plot showing BST1 expression between responders ($n = 13$) and non-responders ($n = 11$) in the Chemo subgroup. **c** Kaplan–Meier analysis demonstrating OS in patients who received chemoimmunotherapy between high expression of BST1 ($n = 12$) and low expression of BST1 ($n = 12$). **d** EFS in patients who received chemoimmunotherapy between high expression of BST1 ($n = 12$) and low expression of BST1 ($n = 12$). **e** ROC curves of BST1 and CDX2 predicting chemoimmunotherapy response. **f** Representative IHC images (5X and 20X) for BST1 of responders and non-responders tumors, scare bar, 200 μm for 5X and 50 μm for 20X image. **g** Bar plot showing BST1 IHC score between responders ($n = 16$) and non-responders ($n = 16$) in the Chemo subgroup. **h** ROC curves of BST1 IHC score predicting chemoimmunotherapy response. **i, j** OS (**i**) and EFS (**j**) in patients who received chemoimmunotherapy between high BST1 IHC score ($n = 16$) and low BST1 IHC score ($n = 16$). **k** GSEA results showing the most significantly enriched pathways in responders and non-responders. Bar length represents normalized enrichment score (NES). **l** Antigen presentation and cytotoxicity enrichment plots from pathway analysis comparing patients with high BST1 expression versus low BST1 expression in the Chemo subgroup. **m, n** Correlation between the BST1 expression level of tumor cell and infiltrated CD8+ T cells (**m**) and NK cells (**n**) based on single-cell RNAseq data (GSE207422). Centers, boxes, whiskers, and dots indicate medians, quantiles, minima/maxima, and outliers, respectively. P value was determined by two-tailed Wald test (**a**), two-tailed Wilcoxon rank sum test (**b**) and two-tailed Student's t test (**g**). Survival data P value was determined by log rank test (**c, d, i, j**). Correlation analyses and P value were performed using one-tailed Spearman's rank tests (**m, n**). GSEA P value was analyzed by empirical phenotype-based permutation test and adjusted P value was adjusted by Benjamini-Hochberg method (**l**). Source data are provided as a Source Data file.

via the broader TCGA dataset. We found no significant differences in *BST1* expression between different races (Supplementary Fig. 4i, j). Moreover, the positive correlation between *BST1* expression and immune infiltration was corroborated by TCGA data for lung adenocarcinoma (LUAD) and lung squamous cell carcinoma (LUSC), which revealed a significant association between *BST1* expression and the infiltration levels of CD8+ T cells and NK cells (Supplementary Fig. 4k–n). However, survival analysis of LUAD and LUSC data from TCGA failed to reveal any prognostic predictive power for BST1 (Supplementary Fig. 4o–p), indicating that BST1 demonstrates specific predictive power for chemoimmunotherapy rather than for chemotherapy alone. Furthermore, using single-cell transcriptomic data from an external neoadjuvant immunotherapy cohort[23]., we found that *BST1* expression on the surface of tumor cells was positively correlated with the abundance of intratumoral CD8 + T cells and NK cells (Fig. 4m, n).

Taken together, our findings strongly reveal the association between *BST1* expression, particularly *BST1* expression on the surface of tumor cells, and immune activation, supporting its role as a promising chemoimmunotherapy biomarker for patients with negative or low-level PD-L1 expression, or in cases where PD-1 status cannot be evaluated.

Anti-tumor immunity was effectively triggered after chemoimmunotherapy in the responders

In responders, we detected specific transcriptional profile alterations after receiving chemoimmunotherapy and multiple immune activation pathways were upregulated (Fig. 5a, b). Furthermore, post-treatment tumor samples from responders presented an elevated immune score and increased infiltration of effective T cells (Fig. 5c–e). This observation implies that chemoimmunotherapy effectively triggers immune cell cytotoxicity within the tumor immune microenvironment (TIME). Concurrently, other immune checkpoint markers were also upregulated post-treatment (Fig. 5f).

Next, we evaluated the TIME between responders and non-responders on the basis of post-treatment tumor sample. We detected distinct transcriptome features between these two groups (Supplementary Fig. 5a). Notably, the pathway "Antigen Processing And Presentation" was found to be significantly enriched in the post-treatment tumor of responders (Supplementary Fig. 5b). Tumor immune cell infiltration and T-cell effectors both indicated that the TIME was not significantly activated in the non-responders, especially for CD8+ T cells, NK cells and NKG7, but not for immunosuppression associated genes (Supplementary Fig. 5c–e).

Discussion

In this phase II umbrella trial, we assessed the feasibility and clinical utility of an anti-PD1 based precision strategy in patients with unresectable stage III NSCLC. Our study aimed to introduce a precise

immunotherapy model for this patient population, emphasizing a targeted approach to minimize reliance on chemotherapy interventions. This trial met its primary endpoint, with 61.7% of patients who underwent surgery having an MPR. Additionally, the PD-L1-positive population in the Chemo-free group had an MPR rate of 55.6%, accompanied by a relatively low treatment-related toxicity. For patients with negative or low-level PD-L1 expression, or in cases where PD-L1 status could not be evaluated, immunotherapy combined with chemotherapy still achieved an excellent MPR rate of 63.2%. Furthermore, exploratory analysis results demonstrated that BST1 are complementary biomarkers to PD-L1 expression, enabling patients to receive more precise combination immunotherapy.

Stage III NSCLC encompasses a heterogeneous patient population, with the majority being ineligible for surgical intervention. In patients with Stage IIIA-B resectable NSCLC, the Neotorch, CheckMate 816, CheckMate 77 T, KEYNOTE-671, and AEGEAN Phase 3 trials revealed that neoadjuvant chemoimmunotherapy during the perioperative period yielded MPR rates ranging from 27.3–48.5% and pCR rates ranging from 10.2–24.8%[7,24–26]. In our trial, despite the inclusion of patients with key poor prognosis indicators (e.g., T4 invasion and bulky/multistation N2 and N3 disease), those who successfully underwent downstaging and surgery achieved a pCR rate of 38.3% and an MPR rate of 61.7%. These findings highlight the potent efficacy of anti-PD1-based precision induction therapy for patients with Stage III unresectable NSCLC.

For patients with unresectable Stage III disease, chemoradiotherapy (CRT) has long been the standard approach for local control. Among patients with driver gene-positive alterations, the LAURA trial reported a 12-month progression-free survival (PFS) rate of 74.0% and a median PFS of 39.1 months for those with EGFR mutations who received CRT followed by osimertinib[27]. Additionally, a global retrospective study reported a 3-year overall survival (OS) rate of 100% for patients with EGFR alterations who received CRT followed by ALK tyrosine kinase inhibitors[28]. For patients without driver gene alterations, novel treatment strategies such as induction, concurrent, and adjuvant immunotherapy are being developed to further improve survival in this specific population[29]. The PACIFIC trial reported an 18-month progression-free survival (PFS) rate of 49.5% and a median PFS of 16.8 months with consolidation durvalumab following cCRT[15]. Similarly, the GEMSTONE-301 trial reported a 12-month PFS rate of 49.5% and a median PFS of 10.5 months with sugemalimab following either cCRT or sequential CRT[30]. However, CRT is associated with increased acute oesophageal toxicity and treatment-related mortality, particularly the lower tolerability of cCRT among East Asian patients[31,32]. Moreover, surgical conversion could represent a crucial step toward a cure by maximizing locoregional control.

In a Phase II trial, neoadjuvant SHR-1701 with chemotherapy followed by surgical conversion provided better event-free survival (EFS) than CRT, with a 12-month EFS rate of 81.5% (95% CI 61.1–91.8) versus
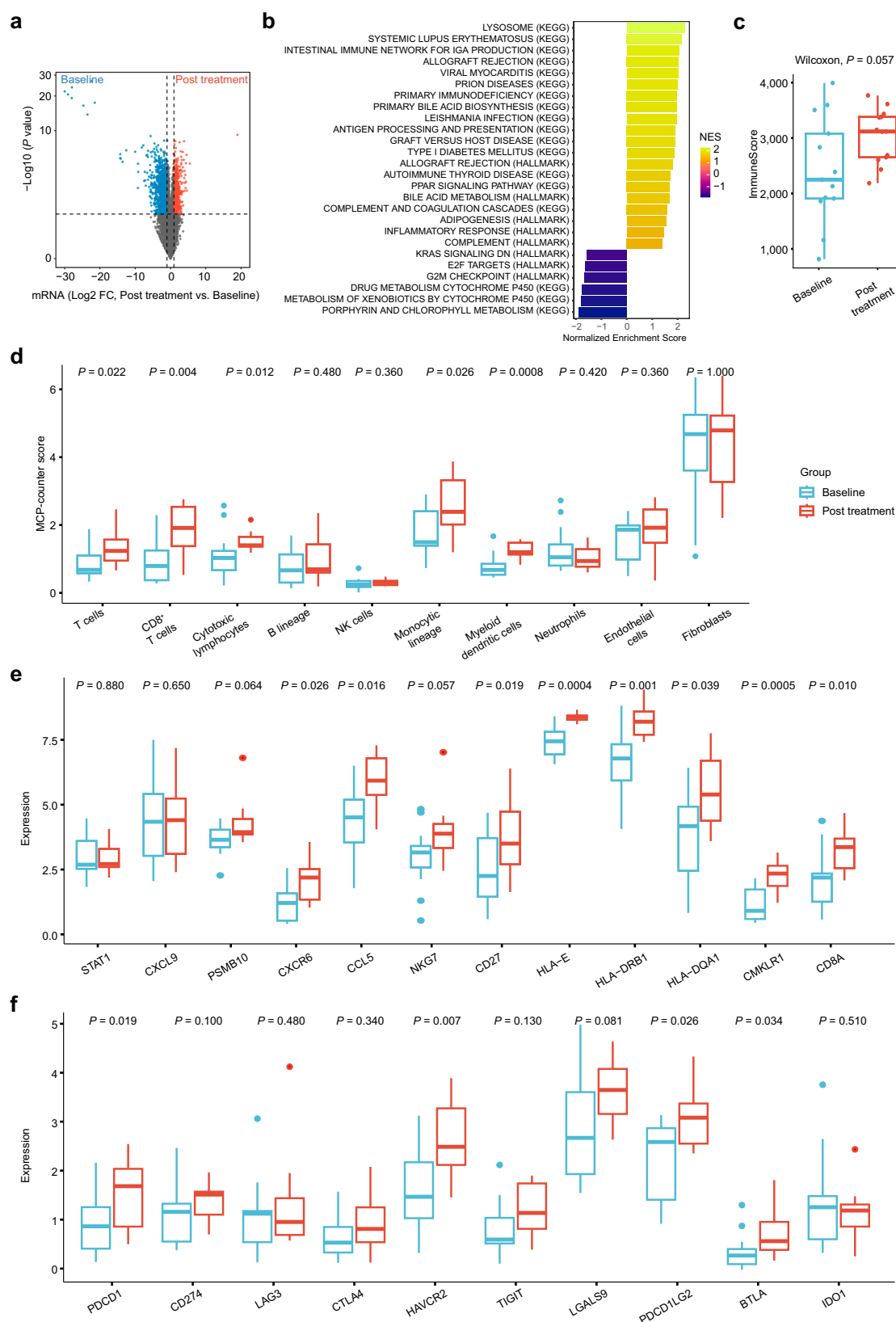
61.3% (95% CI 46.9–72.8)[33]. Several researchers have reported the potential survival benefit of surgery for patients with unresectable NSCLC in the Chinese population[17,34]. Interestingly, our data also indicate that surgical conversion may provide a potential survival benefit for these patients following precise subgroup induction therapy. Nevertheless, despite the favourable survival outcomes observed in the surgical conversion subgroup, caution should be exercised when making cross-subgroup comparisons due to variations in study design, including potential differences in the analysis population for the primary endpoint and patient demographics between arms. Longer-term follow-up and data from standard therapy-controlled trials in different subgroups are needed to fully assess the study regimen.

Fig. 5 | Enhanced activation of the TIME post-treatment in patients responsive to chemoimmunotherapy. a Volcano plot of gene log2 fold change (x-axis) between baseline (*n* = 13) and post treatment (*n* = 13) samples of responders (not paired) in the Chemo subgroup versus -log10 *P* value (y-axis) determined by DEseq2. Points with *P* value < 0.05 and log2 fold change <−1 or >1 are shown in blue and red, respectively. **b** Gene set enrichment analysis (GSEA) results showing the most significantly enriched pathways in responders of Chemo subgroup (post treatment vs. baseline). Bar length represents normalized enrichment score (NES). **c, d** Bar plot showing immune score (**c**) and tumor immune microenvironment infiltration (**d**) between baseline (*n* = 13) and post treatment group (*n* = 13) in the Chemo subgroup responders. **e** Bar plot demonstrating T cell activation related genes expression between baseline (*n* = 13) and post treatment group (*n* = 13) in the Chemo subgroup responders. **f** Bar plot demonstrating immune checkpoints related genes expression between baseline (*n* = 13) and post treatment group (*n* = 13) in the Chemo subgroup responders. Centers, boxes, whiskers, and dots indicate medians, quantiles, minima / maxima, and outliers, respectively. FC, fold change; *P* value as determined by two-tailed Wald test (**a**), two-tailed Wilcoxon rank sum test (**c**–**f**). Source data are provided as a Source Data file.

Pathologic response has been proposed as an early clinical trial endpoint for predicting disease-free and overall survival in neoadjuvant clinical trials of NSCLC[5–8]. However, the evaluation criteria for radiologic responses in these clinical trials remain controversial. Some studies have reported discrepancies between radiologic and pathologic responses. For example, tumors may exhibit pseudo-progression on radiologic imaging in 3% of NSCLC patients, where immune cell infiltration and the inflammatory response are misinterpreted as tumor growth[35]. However, other studies have demonstrated a strong correlation between radiologic and pathologic responses, which is consistent with the findings of our study[16,36]. Nevertheless, further high-quality clinical data are needed to fully address this issue.

The application of antiangiogenic drugs has the potential to modify the TIME, consequently augmenting the efficacy of immunotherapy[37]. Treatment with immunotherapy combined with antiangiogenic agents has become an attractive treatment strategy for solid tumors, including NSCLC[18,38,39]. A Phase II clinical study of the anti-PD-1/VEGF bispecific antibody, AK112, indicated that neoadjuvant treatment with AK112 yielded excellent rates of pathological complete response (pCR) and major pathological response (MPR) (60% and 30%, respectively)[40]. However, in the metastatic NSCLC, it has been demonstrated that the expression status of PD-L1 does not reliably predict the efficacy of anti–PD-(L)1 plus antiangiogenic therapy[39]. In contrast, Zhao et al. highlighted the potential predictive value of high PD-L1 expression for the MPR in patients with resectable NSCLC who received neoadjuvant camrelizumab plus apatinib[18]. In our study, subpopulations that were PD-L1 positive were treated with sintilimab plus IBI305, which yielded promising pathologic results (MPR rate 42.9%). Importantly, the TRAEs observed in the Chemo-free subgroup were significantly lower than those in the Chemo subgroup, thereby enabling patients to effectively adapt to subsequent surgical interventions. Furthermore, previous studies have shown that TMB is a biomarker to estimate survival benefits associated with the combination of ICIs plus anti-VEGFR[39,41]. Similar to previous findings, we found that patients who benefited from immunotherapy plus anti-VEGFR therapy had higher TMB. Despite the limited sample size, we were unable to establish a definitive threshold to distinguish between high and low TMB. However, the findings still provide valuable insights for designing and implementing Phase III clinical trials that investigate "chemotherapy removal" immunotherapy in this highly selective patient population.

Chemotherapy and immunotherapy may have synergistic effects[42,43] and chemotherapy also upregulates PD-L1 expression on tumor cells[44]. However, the effects of chemotherapy on the immune system might also be dose-dependent, adding another element of complexity[45]. In our study, 46.8% of patients in the Chemo subgroup demonstrated resistance to chemoimmunotherapy. Hence, the quest for a more reliable biomarker may enable patients to receive more precise treatment strategies, thereby reducing their reliance on chemotherapy interventions.

BST1 was initially characterized as a surface molecule present in bone marrow stromal cell lines, where it was found to facilitate pre-B-cell growth[46]. Subsequent investigations have improved our understanding, revealing the extensive expression of BST1 in diverse immune cells, such as neutrophils and plasmacytoid dendritic cells[47–49]. Moreover, numerous studies have consistently highlighted BST1 as a central participant in the regulation of critical immune processes, including leukocyte adhesion, migration, and diapedesis via the phosphorylation of Akt and MAPKs[48,50,51]. Our findings also consistently revealed a positive correlation between BST1 expression and the infiltration of CD8^{+} T cells and NK cells. This correlation was consistently observed in both our dataset and the TCGA data. This positive association provides insights into the value of BST1 in assessing the response to chemoimmunotherapy. The exact mechanism underlying how BST1 enhances the efficacy of chemoimmunotherapy remains incompletely understood. However, the identification of this marker provides a direction for exploring innovative therapeutic alternatives to conventional chemotherapy in future research endeavors. We are dedicated to delving deeper into this aspect in subsequent studies.

Given the open-label and single-center nature of this Phase II umbrella trial focused on unresectable Stage III NSCLC patients, caution is warranted when interpreting our results. First, as discussed earlier, the relatively small number of patients in each subgroup raises the potential for over-evaluation of certain conclusions. Secondly, the absence of a directly comparable control group in this non-comparative trial complicates the assessment of the efficacy of each subgroup. Although our data offer valuable perspectives when juxtaposed with historical controls, a more rigorous evaluation is warranted in a phase III randomized clinical trial. Third, a considerable portion of patients in our chemotherapy subgroup lacked detectable PD-L1 expression, which may introduce bias into our results. However, considering the focus of our study on patients with unresectable Stage III NSCLC, we prioritized cytological diagnosis over immunohistochemistry, which enables accurate pathological diagnoses within limited tumor samples[52] and aligns with ethical considerations for clinical management. Fourth, the new biomarker analysis results are exploratory and are based on a limited number of baseline and post-treatment samples. We did not apply multiplicity-adjusted *P* values, which inevitably increases the Type I error rate. In particular, the small sample size of the immunotherapy plus antiangiogenic therapy group restricted our ability to perform a more in-depth analysis that combined RNA and DNA levels. Further exploration of molecular mechanisms and additional clinical trials are imperative for more precise characterization and in-depth exploration of the observed trends. Finally, precision induction immunotherapy provided a good survival benefit. However, the survival data in this study are immature, and whether patients can achieve better long-term survival warrants further follow-up.

In conclusion, the subtyping-based strategy demonstrates promising efficacy with manageable toxicity in patients with unresectable Stage III NSCLC. Our exploratory data provide a more accurate stratification standard based on TMB and BST1 expression, building upon the foundation of stratification by PD-L1 expression and contraindications to antiangiogenic therapy. However, these findings necessitate validation through randomized clinical trials across diverse subgroups. The incorporation of potential predictive biomarkers in future investigations will contribute to a more refined and precise stratification scheme, enhancing our understanding and treatment strategies for patients with unresectable stage III NSCLC.

Methods

Study design

This open-label, single-center, phase II clinical umbrella trial was conducted at Tongji University affiliated Shanghai Pulmonary Hospital, which was registered at https://www.chictr.org.cn/index.html (registration number: ChiCTR2000035367; Fig. S1A). The study was conducted in accordance with the Declaration of Helsinki (as revised in 2013). The study was approved by the independent ethic committee in Tongji University affiliated Shanghai Pulmonary Hospital (L20-335-2). All participants provided written informed consent prior to their inclusion in the study. Informed consent included permission to publish aggregated demographic information, including age, sex distribution, and the medical center involved in the study. To ensure patient confidentiality, any identifiable information has been anonymized in accordance with ethical guidelines and privacy regulations. The demographic data presented reflects the overall distribution of participants, without disclosing any personal identifiers.

Patient eligibility

Between January 21st, 2021, and March 1st, 2023, this study enrolled treatment-naïve participants aged over 18 years with initially unresectable stage III NSCLC (including N2 and N3) according to the 8th edition of the American Joint Committee on Cancer staging manual. Their Eastern Cooperative Oncology Group (ECOG) performance status was 0 or 1. The pathological diagnosis, driver gene mutation status, and PD-L1 expression were confirmed by endobronchial ultrasound (EBUS) or percutaneous lung biopsy. PD-L1 status was determined by immunohistochemical (IHC) staining of PD-L1 protein (clone 22C3) in the submitted tumor samples and categorized as follows: PD-L1 positive was defined as $\geq$ 1% tumor cell membrane staining positive in a minimum of 100 evaluable tumor cells; PD-L1 negative was defined as <1% tumor cell membrane staining positive in a minimum of 100 evaluable tumor cells and PD-L1 not evaluable/indeterminate was defined as participants with insufficient sample quantity or quality to stain for PD-L1 status or those participants in whose samples PD-L1 status could not be determined despite appropriate amounts of tissue sample. Clinical staging was confirmed through positron emission tomography/computed tomography (PET/CT), chest computed tomography (CT), and brain magnetic resonance imaging (MRI). Eligible patients had to exhibit normal hematological indexes as well as qualified hepatic, renal, and pulmonary functions to ensure tolerance for induction therapy followed by radical resection.

Initially unresectable disease was evaluated by MDT, and was defined as (1) pathological confirmed N3 disease; (2) tumor invading vital structures, such as large blood vessels, the trachea, or primary bronchus, with potential for curative resection after tumor downgrading by induction therapy, as judged by a preoperative assessment; (3) clinically confirmed metastatic lymph nodes with multi-station N2 disease or bulky N2 disease, and patients could tolerate hilar and mediastinal lymph node dissection after tumor downgrading by induction therapy as determined by a preoperative evaluation; (4) Possibility of non-R0 resection, even through procedures such as pneumonectomy, specifically right pneumonectomy. The MDT consisted of experts in surgery, radiology, pathology, and oncology. The thoracic surgery specialists had extensive experience, each performing an average of 1,100 thoracic surgeries annually, with over 40 cases involving post-neoadjuvant immunotherapy. All surgeries in this trial were performed by the thoracic surgeons from this MDT team.

Patients with contraindication to IBI305 was defined as per the provided instructions of IBI305, including (1) History of hemoptysis within 3 months prior to screening, with a volume of blood greater than 2.5 mL each time; (2) Symptomatic brain metastases with evidence of hemorrhage; (3) History of myocardial infarction or stroke within 6 months prior to enrollment; (4) History of abdominal fistula, gastrointestinal perforation, or intra-abdominal abscess; (5) Patients who have arterial thrombotic events, esophageal varices, peptic ulcers, wounds, or bone fractures; (6) Radiographic evidence of tumor invasion in great vessels or tumor cavitation.

The exclusion criteria included a history of other malignancies, previous antitumor therapy, severe comorbidities, active autoimmune disease, prior non-infectious pneumonitis, interstitial lung disease, pregnancy or breastfeeding, and EGFR or ALK mutation positive. The detailed inclusion and exclusion criteria are listed in the trial protocol (Supplemental Text 1).

Procedures

Patients who consented to enroll in the trial were assigned to one of these treatment arms based on the expression level of PD-L1 in the primary tumor of patients and whether patients have contraindications to IBI305 (a biosimilar of Bevacizumab). The Treatment subgroups included: (A) immuno-monotherapy for patients with PD-L1 expression level $\geq$ 50% but with contraindications to IBI305; (B) immunotherapy plus anti-angiogenesis therapy for patients with PD-L1 expression level $\geq$ 1% and without contraindications to IBI305 (Chemo-free subgroup: A + B); (C) chemoimmunotherapy for patients with PD-L1 expression level ranging from 1% to 49% but with contraindications to IBI305; (D) chemoimmunotherapy for patients with negative or unknown expression level of PD-L1 (Chemo subgroup: C + D). Sintilimab (200 mg) on day 1 for all participants; IBI305 (15 mg/kg) on day 1 for participants in Treatment-subgroup B; carboplatin (area under curve 5) plus pemetrexed (500 mg/m^2) for participants with adenocarcinoma and carboplatin (area under curve 5) plus nab-paclitaxel (260 mg/m^2) for participants with other pathological subtypes on day 1 in the Chemo subgroup. All participants were scheduled to receive two to four 21-day cycles of induction therapy. Chest CT was performed at the 6th and/or 12th weeks after induction treatment. All CT scans of participants were assessed by the same radiologist and 3 experienced thoracic surgeons via Response Evaluation Criteria in Solid Tumors measurement criteria (RECIST, version 1.1)[53].

After completing two cycles, radiographic assessments and lymph node pathological evaluations (restricted to N3) were conducted. Participants were deemed unresectable if radiographic evaluations (PET/CT, chest CT, or cranial MRI) revealed distant metastasis or tumor invasion into critical structures such as the root of the main vessels, trachea, or other unresectable organs, impacting indispensability. Alternatively, if lymph node pathologic evaluation remained positive in the N3 node, additional treatment cycles were contemplated. For assessing N3 status after induction treatment, patients initially presenting with N3 status underwent reassessment using EBUS or supraclavicular lymph node biopsy. However, sampling challenges, such as difficulty in evaluating stations 5 and 6 lymph nodes, meant that PET/CT results were primarily relied upon. For patients without N3 status prior to induction therapy, PET/CT imaging was primarily employed for assessment. If PET/CT indicated a high suspicion of N3 lymph node involvement, further confirmatory assessments were performed using EBUS or supraclavicular lymph node biopsy to verify potential metastasis. In cases where complete resection was unattainable after four cycles of induction treatment, participants were considered for withdrawal from the study, and their management would transition to an MDT approach. If CR, PR or SD participants after induction could be resected completely, surgery could be performed within 4 - 12 weeks after the induction treatment discontinuation. Adjuvant therapy would be administered 4 to 6 weeks postoperatively, unless the participants were assessed to be unable to tolerate adjuvant therapy or refuses to accept adjuvant treatment. For patients who received chemoimmunotherapy induction therapy, we supplemented the number of chemoimmunotherapy cycles based on the number of cycles they received during induction therapy, ensuring a total of 4 cycles of chemoimmunotherapy. This was followed by one year of maintenance therapy with 17 cycles mono-immunotherapy. For patients who

received chemo-free induction therapy, we recommended 4 cycles of chemoimmunotherapy during the adjuvant therapy period. This was also followed by one year of maintenance therapy with 17 cycles mono-immunotherapy, contingent upon the patient's tolerance to chemotherapy.

Efficacy and safety assessment

The primary endpoint was major pathological response (MPR: ≤ 10% residual viable tumor cells in the primary tumor) rate according to independent pathological review in each arm. The secondary endpoints were pathological response rate (pCR rate, proportion of patients without residual viable tumor cell in the primary tumor and sampled lymph nodes)[54], the objective response rate (ORR), the conversion rate of surgery, event-free survival (EFS, time from initial treatment to any progression of disease [precluding surgery], progression or recurrence of disease after surgery, progression of disease in the absence of surgery, or death from any cause), overall survival (OS, time from treatment assignment to death from any cause), safety and tolerability. Adverse events (AEs) were assessed in all treated patients, with both the assessment and grading of AEs and serious adverse events (SAEs) conducted in accordance with the NCI-CTCAE v5.0 guidelines.

Sample size estimation

The primary endpoint of this research was MPR, which was taken to calculate the sample size. Previous randomized clinical trial reported that the MPR of neoadjuvant chemotherapy for NSCLC at stage IIIA/IIIB was 20% (17/84, P0) in the patients with R0 resection[55]. The null hypothesis (H0) posited that the MPR of anti-PD1-based precision induction therapy would be no greater than 20%, equivalent to the MPR observed with standard neoadjuvant chemotherapy. The MPR for neoadjuvant immune checkpoint inhibitors (ICIs) monotherapy from CheckMate-159 was 45% (9/20)[56], and the MPR of neoadjuvant ICIs plus chemotherapy (LungMate-001) at stage IIIA was 43% (13/30)[36]. Another phase 2 clinical trial revealed the MPR for neoadjuvant ICIs plus anti-VEGFR was 57% (37/65)[18]. Given that the small sample size of these trials may lead to overestimation of the MPR rate, the MPR rate was expected to be 45% (P1) in this study.

It was calculated with α = 0.05 (two-tailed) and the power of test (1-β) = 95%. According to the sample calculation of the one-sample rate test, when P0 = 20%, and P1 = 45%, the sample size will be 42 as calculated for patients with R0 resection. Based on experience from LungMate-001 trial of our hospital (60%, 30 / 50)[36], R0 resection is expected to be achieved in 45% of patients considering the relatively more advanced tumor and lymph node status in this trial. Therefore, 93 patients need to be recruited. Assuming that 5% would drop out early or be lost to follow-up, at least 98 patients will be recruited. According to the study on the proportion of PD-L1 expression level in Chinese population, the expression level of PD-L1 ≥ 50% accounted for 11.4%, 1-49% accounted for 22.4%, and <1% accounted for 66.3%[57]. Because the determination of PD-L1 expression depends on the amount of tissue punctured, the tumor tissue obtained by puncture in some patients is too small to be determined. The experience of thoracic surgery department in our hospital accounts for about 40% (98*40% = 39 patients)[16,36]. Therefore, it is expected that at least 20 patients (7 [98*60%*11.4%] + 13 [98*60%*22.4%]) will be enrolled in Chemo-free subgroup, and at least 78 (39 [98*60%*66.3%] + 39) will be enrolled in Chemo subgroup.

Follow-up

Follow-up was acquired by telephone contact or outpatient visit. For surgical treated participants, chest CT were performed every 3 months for the first year postoperatively, every 6 months for 2 to 5 years, and annually from then on. MRI of the brain, ultrasonography of abdominal regions, bone scans were performed annually. Local recurrence was defined as the recurrence in the primary site or mediastinal lymph nodes, while distant recurrence was defined as recurrence in other sites. The follow-up was conducted until death.

Exploratory analysis

The distribution of PD-L1 expression in the intention-to-treat analysis were examined. Additionally, other potential predictive biomarkers, such as gene expression profiling, tumor mutational burden, and infiltration of immune cells into archived and/or fresh tumor tissue, were evaluated either prior to or after surgery during the course of the study treatment. Furthermore, their correlation with disease status and/or therapeutic efficacy was assessed. These analyses were pre-specified in the approved study protocol.

RNA sequencing and data processing

Total RNA from fresh frozen tissues was extracted with TRIzol (Invitrogen, 15596026). Sequencing libraries were generated using a NEB-Next Ultra RNA Library Prep Kit for Illumina (NEB, E7770), and index codes were added to attribute sequences to each sample. The libraries were pooled, and paired-end sequencing (2×150 bp reads) was performed using an Illumina NovaSeq 6000. After RNAseq sequencing, raw fastq files were trimmed via fastp (v0.20.1)[58] and aligned to GRCh38 reference genome by STAR (v2.7.6a)[59] with default settings. After obtaining the BAM files, read counts were summarized by featureCounts (v2.0.1)[60]. TPMs (Trans Per Million) were generated using Salmon (v0.6.0)[61]. Batch effects were adjusted using "combat" function in sva package[62].

Differentially expressed gene analysis

We used DESeq2 to calculate differential gene expression between sample groups[63]. The DESeq2 profiles genes according to model gene count expression data and calculates |Log2Fold Change|, which estimates the effect size and represents gene changes between comparison groups. The two-sided Wald-test statistics are computed to exam the differential expression across the comparison groups. Genes with |Log2Fold Change| > 1 and Wald test $P < 0.05$ were defined as differentially expressed genes. We used volcano plots to visualize the differential gene expression results.

Gene set enrichment analysis

For gene set enrichment analysis (GSEA) analysis, results for all protein coding genes were ranked by Log2fold change and evaluated with the "GSEA" algorithm[64]. "Hallmark" and "KEGG" gene sets were acquired from MSigDb. We filtered GSEA result based on the criteria that the P-value <0.05 and visualized the pathways as candidates based on the normalized enrichment score.

Tumor micro-environment estimation

The immune scores of each sample were calculated using the "ESTI-MATE" R package[65]. The infiltration of immune cells was evaluated by "mcpcounter" (v1.2.0)[66].

TCGA data analysis

The correlation between expression of BST1 and tumor micro-environment immune infiltration was conducted by TIMER2.0 (http://timer.comp-genomics.org/timer/)[67]. Additionally, the correlation between the expression of BST1 in lung cancer (LUAD plus LUSC) was analyzed by GEPIA[68].

DNA sequencing and data processing

In this study, 35 baseline samples were collected and successfully conducted for DNA sequencing. According to the manufacturer's protocol, genomic DNA was extracted from tumors using QIAamp Fast DNA tissue kit (QIAGEN). Total DNA was quantified by the Qubit 2.0 Flurometer (Life Technologies) and NanoDrop 2000 (Thermo Fisher

Scientific) and the integrity was assessed by TapeStation (Agilent Technologies). For Illumina sequencing library construction, the genomic DNA was fragmented to an average size of 180-280 bp using a Covaris focused-ultrasonicator. Then, WES libraries were prepared and captured using the Agilent SureSelect Human All Exon V6 kit (Agilent Technologies, 5190-8865) following the manufacturer's instructions. The DNA library with 150 bp paired-end reads was sequenced on the Illumina Novaseq 6000 platform.

To detect single nucleotide variant (SNV) and small insertion/deletion (INDEL), the GATK (v4.0.6.0) best practice guideline was followed[69]. After excluding low-quality reads, qualified paired-end WES sequencing reads were aligned to human reference genome (hg38) with BWA MEM (v0.7.15)[70]. The resulting BAM files were further processed with Picard tools to remove PCR duplicates. SNVs and INDELs were detected using MuTect2 in tumor-only mode with panel-of-normals[71]. Then we filtered out short tandem repeat regions downloaded from UCSC table browser, and finally annotated using Funcotator from GATK. Oncoplot was plotted using "Maftools" R package[72].

Immunohistochemistry analysis

Tumor tissues were fixed in 10% neutral buffered formalin, embedded into paraffin blocks, cut into 4 - 5 μm slides. The tumor samples were provided by the Pathology Department of Shanghai Pulmonary Hospital. The slides were stained with Anti-BST1 antibody (Abcam: ab137718, dilusion:1/100) and nuclei were stained with hematoxylin dye. At last the sections were scanned using the Pannoramic 250/ MIDI. The immunohistochemical (IHC) score were determined in five randomly selected areas. The staining results were semi-quantitatively evaluated by the multiply of staining intensity and the percentage of positive staining cells[73]. The percentage of positive cells was given into four grades by ImageJ: 0 for <5%; 1 for 6%–25%; 2 for 26%–50%; 3 for 51%–75% and 4 for >75%. Staining intensity was assessed by four degrees: 0, negative; 1, weak; 2, moderate; and 3, strong. The intensity was assessed by IHC Profiler[74].

Single-cell RNA sequencing analysis

To explore the association between BST1 and immune cells, we used the single-cell RNAseq data of immunochemotherapy from our previous study[23]. The data processing, cell clustering, annotation and tumor cell identification have been described in previous study. The mean value of BST1 in tumor cells was calculated for each sample. Then, we calculated the cellular fraction for each immune lineage in all CD45+ cells. Notably, to avoid the bias caused by inaccurate estimations, samples with less than 10 cells were excluded for calculating cellular factions and average gene expression. Spearman correlation test was performed to test correlation between BST1 expression and the cellular fraction.

Statistical analysis & reproducibility

Considering that our study population consists of patients with stage III initially unresectable NSCLC, including patients who did not convert to resectable status and received surgery in the effectiveness analysis may introduce selection bias. The pathological effectiveness of the treatment was evaluated based on patients who had comprehensive pathological assessment reports from our hospital. Patients who were deemed resectable but discontinued the trial for reasons other than disease progression were excluded from the primary analysis.

Additionally, to better demonstrate the real-world impact of precise stratification of induction therapy in patients with stage III initially unresectable NSCLC, further analyses of ORR, survival, and safety were conducted using the ITT population who had received at least one dose of induction therapy. The 95% CIs of MPR rate, pCR rate and ORR were estimated by means of the Clopper-Pearson method. Time-to-event analyses were estimated with the Kaplan–Meier method, with median survival time presented with 95% CIs based on

the Brookmeyer-Crowley method and survival rates presented along with 95% CIs based on the complementary log-log transformation method. The median follow-up time was determined using the reverse Kaplan-Meier method. TRAEs were summarized with frequencies (percentages). Additionally, EFS and OS stratified by surgery were explored by post-hoc analyses.

Wilcoxon test was applied to compare the expression differences between sample groups. To separate patients into low- or high-BST1 expression groups, the cutoff was generated based on the association between gene expression and survival data using the survminer package. All P values were two-sided, with $P < 0.05$ considered statistically significant. Statistical analyses were conducted using R programming (version 4.3.1).

Reporting summary

Further information on research design is available in the Nature Portfolio Reporting Summary linked to this article.

Data availability

All data generated and supporting the findings of this study are available within the paper. The trial protocol and statistical analysis plan can be found in the Supplementary Information. The transcriptomic sequencing and whole exomes sequencing data have been submitted to the Genome Sequence Archive database under accession number HRA006345. The sequencing data are available under controlled access due to data privacy laws related to patient consent for data sharing and the data should be used for research purposes only. Access can be obtained by approval via the Data Access Committee in the GSA-human database. The approximate response time for accession requests is about 2 weeks. Once access has been granted, the data will be available to download for 3 months. Clinical data are not publicly available due to involving patient privacy, but can be accessed from the corresponding author Peng Zhang (Email: zhang-peng1121@tongji.edu.cn), upon request for 3 years; individual de-identified patient data will be shared for clinical study analyses. Source data are provided with this paper.

Code availability

No new algorithms were developed for this study. However, all codes used in this study are immediately available from the corresponding author upon request.

References

1. Bray, F. et al. Global cancer statistics 2022: GLOBOCAN estimates of incidence and mortality worldwide for 36 cancers in 185 countries. *CA Cancer J. Clin.* **74**, 229–263 (2024).
2. Goldstraw, P. et al. The IASLC Lung Cancer Staging Project: Proposals for Revision of the TNM Stage Groupings in the Forthcoming (Eighth) Edition of the TNM Classification for Lung Cancer. *J. Thorac. Oncol.* **11**, 39–51 (2016).
3. Arbour, K. C. & Riely, G. J. Systemic Therapy for Locally Advanced and Metastatic Non-Small Cell Lung Cancer: A Review. *Jama* **322**, 764–774 (2019).
4. Simone, C. B. et al. ASTRO Radiation Therapy Summary of the ASCO Guideline on Management of Stage III Non-Small Cell Lung Cancer. *Pr. Radiat. Oncol.* **13**, 195–202 (2023).
5. Forde, P. M. et al. Neoadjuvant Nivolumab plus Chemotherapy in Resectable Lung Cancer. *N. Engl. J. Med.* **386**, 1973–1985 (2022).
6. Cascone, T., e.a. CheckMate 77T: Phase III study comparing neoadjuvant nivolumab (NIVO) plus chemotherapy (chemo) vs neoadjuvant placebo plus chemo followed by surgery and adjuvant NIVO or placebo for previously untreated, resectable stage II–IIIb NSCLC. in ESMO Congress *2023* (LBA1).
7. Wakelee, H. et al. Perioperative Pembrolizumab for Early-Stage Non-Small-Cell Lung Cancer. *N. Engl. J. Med.* **389**, 491–503 (2023).

8. Lu, S. et al. Perioperative toripalimab + platinum-doublet chemotherapy vs chemotherapy in resectable stage II/III non-small cell lung cancer (NSCLC): Interim event-free survival (EFS) analysis of the phase III NEOTORCH study. *J. Clin. Oncol.* **41**, 8501–8501 (2023).

9. Reck, M. et al. Pembrolizumab versus Chemotherapy for PD-L1-Positive Non-Small-Cell Lung Cancer. *N. Engl. J. Med.* **375**, 1823–1833 (2016).

10. Gandhi, L. et al. Pembrolizumab plus Chemotherapy in Metastatic Non-Small-Cell Lung Cancer. *N. Engl. J. Med.* **378**, 2078–2092 (2018).

11. Paz-Ares, L. et al. Pembrolizumab plus Chemotherapy for Squamous Non-Small-Cell Lung Cancer. *N. Engl. J. Med.* **379**, 2040–2051 (2018).

12. Hendriks, L. E. et al. Non-oncogene-addicted metastatic non-small-cell lung cancer: ESMO Clinical Practice Guideline for diagnosis, treatment and follow-up. *Ann. Oncol.* **34**, 358–376 (2023).

13. Ettinger, D. S. et al. Non-Small Cell Lung Cancer, Version 3.2022, NCCN Clinical Practice Guidelines in Oncology. *J. Natl Compr. Canc. Netw.* **20**, 497–530 (2022).

14. Spigel, D. R. et al. Five-Year Survival Outcomes From the PACIFIC Trial: Durvalumab After Chemoradiotherapy in Stage III Non-Small-Cell Lung Cancer. *J. Clin. Oncol.* **40**, 1301–1311 (2022).

15. Antonia, S. J. et al. Durvalumab after Chemoradiotherapy in Stage III Non-Small-Cell Lung Cancer. *N. Engl. J. Med.* **377**, 1919–1929 (2017).

16. Zhu, X. et al. Safety and effectiveness of neoadjuvant PD-1 inhibitor (toripalimab) plus chemotherapy in stage II-III NSCLC (LungMate 002): an open-label, single-arm, phase 2 trial. *BMC Med.* **20**, 493 (2022).

17. Deng, H. et al. Radical Minimally Invasive Surgery After Immunochemotherapy in Initially-unresectable Stage IIIB Non-small cell Lung Cancer. *Ann. Surg.* **275**, e600–e602 (2022).

18. Zhao, J. et al. Efficacy, Safety, and Biomarker Analysis of Neoadjuvant Camrelizumab and Apatinib in Patients With Resectable NSCLC: A Phase 2 Clinical Trial. *J. Thorac. Oncol.* **18**, 780–791 (2023).

19. Hegde, P. S., Wallin, J. J. & Mancao, C. Predictive markers of anti-VEGF and emerging role of angiogenesis inhibitors as immunotherapeutics. *Semin. Cancer Biol.* **52**, 117–124 (2018).

20. Chen, D. S. & Mellman, I. Oncology meets immunology: the cancer-immunity cycle. *Immunity* **39**, 1–10 (2013).

21. Voron, T. et al. VEGF-A modulates expression of inhibitory checkpoints on CD8+ T cells in tumors. *J. Exp. Med.* **212**, 139–148 (2015).

22. Badia-Ramentol, J. et al. The prognostic potential of CDX2 in colorectal cancer: Harmonizing biology and clinical practice. *Cancer Treat. Rev.* **121**, 102643 (2023).

23. Hu, J. et al. Tumor microenvironment remodeling after neoadjuvant immunotherapy in non-small cell lung cancer revealed by single-cell RNA sequencing. *Genome Med.* **15**, 14 (2023).

24. Lu, S. et al. Perioperative Toripalimab Plus Chemotherapy for Patients With Resectable Non-Small Cell Lung Cancer: The Neotorch Randomized Clinical Trial. *Jama* **331**, 201–211 (2024).

25. Cascone, T. et al. LBA1 CheckMate 77T: Phase III study comparing neoadjuvant nivolumab (NIVO) plus chemotherapy (chemo) vs neoadjuvant placebo plus chemo followed by surgery and adjuvant NIVO or placebo for previously untreated, resectable stage II–IIIb NSCLC. *Ann. Oncol.* **34**, S1295 (2023).

26. Heymach, J. V. et al. Perioperative Durvalumab for Resectable Non-Small-Cell Lung Cancer. *N. Engl. J. Med.* **389**, 1672–1684 (2023).

27. Lu, S. et al. Osimertinib after Chemoradiotherapy in Stage III EGFR-Mutated NSCLC. *N. Engl. J. Med.* **391**, 1555 (2024).

28. Jayakrishnan, R. et al. Global retrospective study comparing consolidation ALK tyrosine kinase inhibitors (TKI) to durvalumab (durva) or observation (obs) after chemoradiation (CRT) in unresectable locally-advanced ALK+ non-small cell lung cancer (NSCLC). *J. Clin. Oncol.* **42**, 8013 (2024).

29. Cortiula, F. et al. Immunotherapy in unresectable stage III non-small-cell lung cancer: state of the art and novel therapeutic approaches. *Ann. Oncol.* **33**, 893–908 (2022).

30. Zhou, Q. et al. Sugemalimab versus placebo after concurrent or sequential chemoradiotherapy in patients with locally advanced, unresectable, stage III non-small-cell lung cancer in China (GEMSTONE-301): interim results of a randomised, double-blind, multicentre, phase 3 trial. *Lancet Oncol.* **23**, 209–219 (2022).

31. Aupérin, A. et al. Meta-analysis of concomitant versus sequential radiochemotherapy in locally advanced non-small-cell lung cancer. *J. Clin. Oncol.* **28**, 2181–2190 (2010).

32. O'Rourke, N. & Macbeth, F. Is concurrent chemoradiation the standard of care for locally advanced non-small cell lung cancer? A review of guidelines and evidence. *Clin. Oncol. (R. Coll. Radio.)* **22**, 347–355 (2010).

33. Zhou, Q. et al. Neoadjuvant SHR-1701 with or without chemotherapy in unresectable stage III non-small-cell lung cancer: A proof-of-concept, phase 2 trial. *Cancer Cell* **42**, 1258–1267.e1252 (2024).

34. Zheng, J. et al. Efficacy and surgical safety of sequential surgical resection after pembrolizumab plus chemotherapy for initial unresectable stage IIIB non-small cell lung cancer. *Lung Cancer* **184**, 107326 (2023).

35. Fujimoto, D. et al. Pseudoprogression in Previously Treated Patients with Non-Small Cell Lung Cancer Who Received Nivolumab Monotherapy. *J. Thorac. Oncol.* **14**, 468–474 (2019).

36. Zhang, P. et al. Neoadjuvant Sintilimab and Chemotherapy for Resectable Stage IIIA Non-Small Cell Lung Cancer. *Ann. Thorac. Surg.* **114**, 949–958 (2022).

37. Huinen, Z. R., Huijbers, E. J. M., van Beijnum, J. R., Nowak-Sliwinska, P. & Griffioen, A. W. Anti-angiogenic agents - overcoming tumour endothelial cell anergy and improving immunotherapy outcomes. *Nat. Rev. Clin. Oncol.* **18**, 527–540 (2021).

38. Socinski, M. A. et al. Atezolizumab for First-Line Treatment of Metastatic Nonsquamous NSCLC. *N. Engl. J. Med.* **378**, 2288–2301 (2018).

39. Provencio, M. et al. Atezolizumab Plus Bevacizumab as First-line Treatment for Patients With Metastatic Nonsquamous Non-Small Cell Lung Cancer With High Tumor Mutation Burden: A Non-randomized Controlled Trial. *JAMA Oncol.* **9**, 344–353 (2023).

40. Changli, W. et al. A Phase II Study of Perioperative Ivonescimab Alone or Combined with Chemotherapy in Resectable Non-Small Cell Lung Cancer. Vol. OA01.06 (WCLC, 2024).

41. Rousseau, B. et al. The Spectrum of Benefit from Checkpoint Blockade in Hypermutated Tumors. *N. Engl. J. Med.* **384**, 1168–1170 (2021).

42. Gaudreau, P. O. et al. Neoadjuvant Chemotherapy Increases Cytotoxic T Cell, Tissue Resident Memory T Cell, and B Cell Infiltration in Resectable NSCLC. *J. Thorac. Oncol.* **16**, 127–139 (2021).

43. Jackaman, C., Majewski, D., Fox, S. A., Nowak, A. K. & Nelson, D. J. Chemotherapy broadens the range of tumor antigens seen by cytotoxic CD8(+) T cells in vivo. *Cancer Immunol. Immunother.* **61**, 2343–2356 (2012).

44. Ock, C. Y. et al. Changes in programmed death-ligand 1 expression during cisplatin treatment in patients with head and neck squamous cell carcinoma. *Oncotarget* **8**, 97920–97927 (2017).

45. He, X. et al. Upfront dose-reduced chemotherapy synergizes with immunotherapy to optimize chemoimmunotherapy in squamous cell lung carcinoma. *J. Immunother. Cancer* **8**, e000807 (2020).

46. Kaisho, T. et al. BST-1, a surface molecule of bone marrow stromal cell lines that facilitates pre-B-cell growth. *Proc. Natl. Acad. Sci. USA* **91**, 5325–5329 (1994).

47. Ishihara, K. et al. Stage-specific expression of mouse BST-1/BP-3 on the early B and T cell progenitors prior to gene rearrangement of antigen receptor. *Int. Immunol.* **8**, 1395–1404 (1996).

48. Funaro, A. et al. CD157 is an important mediator of neutrophil adhesion and migration. *Blood* **104**, 4269–4278 (2004).

49. Hernández-Campo, P. M., Almeida, J., Sánchez, M. L., Malvezzi, M. & Orfao, A. Normal patterns of expression of glycosylphosphatidylinositol-anchored proteins on different subsets of peripheral blood cells: a frame of reference for the diagnosis of paroxysmal nocturnal hemoglobinuria. *Cytom. B Clin. Cytom.* **70**, 71–81 (2006).

50. Ortolan, E. et al. CD157 plays a pivotal role in neutrophil transendothelial migration. *Blood* **108**, 4214–4222 (2006).

51. Lo Buono, N. et al. The CD157-integrin partnership controls transendothelial migration and adhesion of human monocytes. *J. Biol. Chem.* **286**, 18681–18691 (2011).

52. Lau, S. C. M. et al. PD-L1 assessment in cytology samples predicts treatment response to checkpoint inhibitors in NSCLC. *Lung Cancer* **171**, 42–46 (2022).

53. Eisenhauer, E. A. et al. New response evaluation criteria in solid tumours: revised RECIST guideline (version 1.1). *Eur. J. Cancer* **45**, 228–247 (2009).

54. Travis, W. D. et al. IASLC Multidisciplinary Recommendations for Pathologic Assessment of Lung Cancer Resection Specimens After Neoadjuvant Therapy. *J. Thorac. Oncol.* **15**, 709–740 (2020).

55. Thomas, M. et al. Effect of preoperative chemoradiation in addition to preoperative chemotherapy: a randomised trial in stage III non-small-cell lung cancer. *Lancet Oncol.* **9**, 636–648 (2008).

56. Forde, P. M. et al. Neoadjuvant PD-1 Blockade in Resectable Lung Cancer. *N. Engl. J. Med.* **378**, 1976–1986 (2018).

57. Fu, F. et al. Distribution and concordance of PD-L1 expression by routine 22C3 assays in East-Asian patients with non-small cell lung cancer. *Respir. Res.* **23**, 302 (2022).

58. Chen, S., Zhou, Y., Chen, Y. & Gu, J. fastp: an ultra-fast all-in-one FASTQ preprocessor. *Bioinformatics* **34**, i884–i890 (2018).

59. Dobin, A. et al. STAR: ultrafast universal RNA-seq aligner. *Bioinformatics* **29**, 15–21 (2013).

60. Liao, Y., Smyth, G. K. & Shi, W. featureCounts: an efficient general purpose program for assigning sequence reads to genomic features. *Bioinformatics* **30**, 923–930 (2014).

61. Patro, R., Duggal, G., Love, M. I., Irizarry, R. A. & Kingsford, C. Salmon provides fast and bias-aware quantification of transcript expression. *Nat. Methods* **14**, 417–419 (2017).

62. Ge, D. et al. SVA: software for annotating and visualizing sequenced human genomes. *Bioinformatics* **27**, 1998–2000 (2011).

63. Love, M. I., Huber, W. & Anders, S. Moderated estimation of fold change and dispersion for RNA-seq data with DESeq2. *Genome Biol.* **15**, 550 (2014).

64. Subramanian, A. et al. Gene set enrichment analysis: a knowledge-based approach for interpreting genome-wide expression profiles. *Proc. Natl. Acad. Sci. USA* **102**, 15545–15550 (2005).

65. Yoshihara, K. et al. Inferring tumour purity and stromal and immune cell admixture from expression data. *Nat. Commun.* **4**, 2612 (2013).

66. Becht, E. et al. Estimating the population abundance of tissue-infiltrating immune and stromal cell populations using gene expression. *Genome Biol.* **17**, 218 (2016).

67. Li, T. et al. TIMER2.0 for analysis of tumor-infiltrating immune cells. *Nucleic Acids Res.* **48**, W509–w514 (2020).

68. Tang, Z. et al. GEPIA: a web server for cancer and normal gene expression profiling and interactive analyses. *Nucleic Acids Res.* **45**, W98–w102 (2017).

69. DePristo, M. A. et al. A framework for variation discovery and genotyping using next-generation DNA sequencing data. *Nat. Genet.* **43**, 491–498 (2011).

70. Li, H. & Durbin, R. Fast and accurate short read alignment with Burrows-Wheeler transform. *Bioinformatics* **25**, 1754–1760 (2009).

71. Cibulskis, K. et al. Sensitive detection of somatic point mutations in impure and heterogeneous cancer samples. *Nat. Biotechnol.* **31**, 213–219 (2013).

72. Mayakonda, A., Lin, D. C., Assenov, Y., Plass, C. & Koeffler, H. P. Maftools: efficient and comprehensive analysis of somatic variants in cancer. *Genome Res.* **28**, 1747–1756 (2018).

73. Xu, Q. et al. MicroRNA-1296 inhibits metastasis and epithelial-mesenchymal transition of hepatocellular carcinoma by targeting SRPK1-mediated PI3K/AKT pathway. *Mol. Cancer* **16**, 103 (2017).

74. Varghese, F., Bukhari, A. B., Malhotra, R. & De, A. IHC Profiler: an open source plugin for the quantitative evaluation and automated scoring of immunohistochemistry images of human tissue samples. *PLoS One* **9**, e96801 (2014).

Acknowledgements

Author contributions

P.Z., L.Z., J.D., and D.X. conceived and designed the trial; Y.Yang, Y.Zhao, X.L., N.S., L.D., and W.H. provided the materials and patients support. Y.Zhu, D.Z., and G.J. provided the administrative support; C.Y., D.B., S.W., Z.S., and H.Y. collected the data; C.Y., D.B., J.W., S.H., L.S., and Y.Yan. performed data analysis; C.Y., L.W., J.Z., and L.Z. conducted all the experiments and performed the statistical analysis of the data; C.Y., L.Z., D.B., J.W., S.H., L.S., and Y.Yan wrote the manuscripts; P.Z., L.Z., J.D., and D.X. drafted the manuscript. All authors discussed the experiments and results and approved the manuscript.

Competing interests

The authors declare no competing interests.

Inclusion and diversity

We support inclusive, diverse, and equitable conduct of research.

Additional information

Supplementary information The online version contains supplementary material available at https://doi.org/10.1038/s41467-025-57184-z.

Correspondence and requests for materials should be addressed to Dong Xie, Jie Dai, Lele Zhang or Peng Zhang.

Peer review information *Nature Communications* thanks Oscar Arrieta, who co-reviewed with Luis Lara-Mejia, and Federico Cappuzzo, Joshua Savage, the other, anonymous, reviewer(s) for their contribution to the peer review of this work. A peer review file is available.

Reprints and permissions information is available at http://www.nature.com/reprints